Direct Observation of the Formation of Polar Nanoregions in $Pb(Mg_{1/3}Nb_{2/3})O_3$ Using Neutron Pair Distribution Function Analysis

I.-K. Jeong,* T. W. Darling, J. K. Lee, Th. Proffen, and R. H. Heffner

Los Alamos National Laboratory, Los Alamos, New Mexico 87545, USA

J. S. Park and K. S. Hong

School of Materials Science and Engineering, Seoul National University, Seoul, Korea

W. Dmowski

Department of Materials Science and Engineering, University of Tennessee, Knoxville, Tennessee 37996, USA

T. Egami

Department of Materials Science and Engineering and Department of Physics and Astronomy, University of Tennessee, Knoxville, Tennessee 37996, USA, and Oak Ridge National Laboratory, Oak Ridge, Tennessee 37831, USA

Using neutron pair distribution function analysis over the temperature range from 1000 to 15 K, we demonstrate the existence of local polarization and the formation of medium-range, polar nanoregions (PNRs) with local rhombohedral order in a prototypical relaxor ferroelectric $Pb(Mg_{1/3}Nb_{2/3})O_3$. We estimate the volume fraction of the PNRs as a function of temperature and show that this fraction steadily increases from 0% to a maximum of $\sim 30\%$ as the temperature decreases from 650 to 15 K. Below $T \sim 200$ K the volume fraction of the PNRs becomes significant, and PNRs freeze into the spin-glass-like state.

Relaxor ferroelectrics, such as lead magnesium niobate $Pb(Mg_{1/3}Nb_{2/3})O_3$ (PMN), have been widely applied due to their high, relatively temperature-independent permittivities. Relaxors are characterized by a frequency dispersion in their maximum permittivity temperature ($T_M \sim 285$ K in PMN), with no macroscopic phase transition into a ferroelectric state at T_M [1]. These behaviors are fundamentally different from those of normal ferroelectrics and are similar to spin glasses [2]. It is now believed that local polarization, resulting from structural and chemical disorder, plays a crucial role in relaxor behavior [3,4]. Several models have been proposed to explain the nature of the interactions between these local polarizations and the mechanism for relaxor behavior [3,5–9]. These models include superparaelectric [3,5] and dipole glasses [6], as well as random field interactions [7]. The microscopic mechanism behind relaxor ferroelectricity is, however, not fully understood, and is still controversial due to its high degree of complexity.

In this Letter, we report the temperature evolution of the local and medium-range crystal structure of PMN from 1000 to 15 K using neutron pair distribution function (PDF) analysis. We present evidence for both local atomic displacements (local polarization) and for medium-range (~ 5–50 Å) ordering, called polar nanoregions (PNRs). These medium-range correlations are modeled using rhombohedral symmetry, enabling for the first time an estimate of the temperature dependence of the volume fraction of the PNRs. This fraction increases with decreas-

ing temperature, reaching the three-dimensional percolation threshold below $T \sim 200$ K, where the PNRs start to overlap. We discuss the implications of these findings on the dielectric properties of PMN.

Evidence for the existence of local polarization in PMN below $T_d \sim 620$ K, known as the Burns temperature [4], was deduced from optical and strain measurements [3,10,11]. The atomic nature of this polarization in PMN was also studied using extended x-ray absorption fine structure (EXAFS) [12,13] and atomic PDF analysis [14,15]. Niobium K-edge EXAFS measurements on PMN suggested a displacement of Nb ions with respect to their oxygen octahedra by about 0.1 Å from room temperature down to 4.5 K. Lead K-edge EXAFS measurements indicated strong disorder on the Pb sites, but provided no detailed information about Pb displacements [12]. This is in contrast to neutron PDF measurements on PMN which clearly showed that the Pb ions are off centered with respect to the O_{12} cage by as much as 0.5 Å [14,15]. In these earlier PDF measurements, however, a complete picture of local structure in PMN was not obtained due to the limited Q resolution and temperature range studied. Thus, the nature of PNRs and their volume fraction were not determined.

Our measurements were performed on the NPDF instrument at the Los Alamos Neutron Science Center (LANSCE). Powder diffraction patterns were corrected for background, absorption, and multiple scattering, and normalized using a vanadium spectrum to obtain the total

scattering structure function $S(Q)$, using the PDFGETN program [16]. The PDF $G(r)$ is obtained from $S(Q)$ via the Fourier transform shown in Eq. (1),

$$G(r) = 4\pi r[\rho(r) - \rho_0]$$
$$= \frac{2}{\pi} \int_0^{Q_{max}} Q[S(Q) - 1]\sin Qr\, dQ, \qquad (1)$$

where $\rho(r)$ and ρ_0 are the atomic pair number density and average number density, respectively. Since $S(Q)$ includes both Bragg and diffuse scattering, the resultant PDF provides short-, medium-, and long-range structural information [17]. This technique has been used to study local atomic structures [17,18] and correlated atomic motions of atom pairs [19] in many materials.

We first examine the temperature evolution of the low-r region of the PDF spectra. Figure 1(a) shows spectra from 1000 to 313 K. The tick marks indicate the PDF peak positions for an ideal cubic perovskite structure. The first tick mark represents Mg/Nb-O, the second Pb-O, O-O, the third Mg/Nb-Pb, and the fourth Pb-Pb, O-O, Mg/Nb-Mg/Nb bond lengths. At high temperatures, note that the peaks are quite broad and the Pb-Mg/Nb bond is not well defined due to an overlap with the Pb-O bond. As the temperature decreases to room temperature, a shoulder appears around ~2.5 Å. This splitting indicates
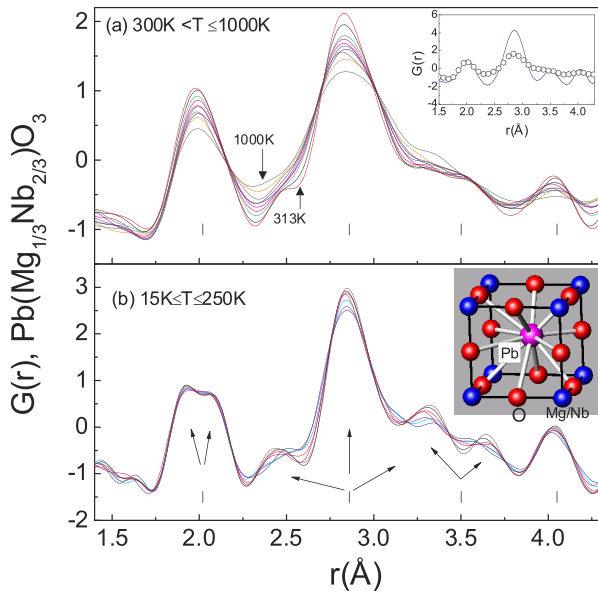

FIG. 1 (color online).   Temperature evolution of PDF spectra of PMN within a unit cell. (a) High temperature: $T = 1000$, 850, 750, 700, 650, 600, 550, 500, 400, and 313 K, with $Q_{max} = 25$ Å^{-1}. The inset shows a comparison between an experimental PDF (symbols) and a model PDF (line) at 650 K. See text for details. (b) Low temperature: $T = 250$, 220, 190, 150, 100, 50, and 15 K, with $Q_{max} = 30$ Å^{-1}. The tick marks indicate (from left to right, respectively) Mg/Nb-O, (Pb-O, O-O), Mg/Nb-Pb, and (Pb-Pb, O-O, Mg/Nb-Mg/Nb) bond lengths in an ideal cubic perovskite structure of PMN. The inset shows the cubic crystal structure with the Pb ion at body center.

a displacement of Pb ions in their O_{12} cages, which breaks 12-fold degeneracy of the Pb-O bond distance [see the inset of Fig. 1(b)] [20].

In order to understand the origin of these phenomena, we compared the experimental PDF at 650 K with a model PDF at the same temperature [shown in the inset of Fig. 1(a)]. In the model PDF we assumed no atomic displacements and calculated the widths using thermal parameters for Pb, Mg/Nb, and O ions obtained from our Rietveld refinement at 650 K. Since the area of the Pb-O peak should be conserved, the comparison shown in the inset of Fig. 1(a) indicates that the Pb-O peak is much broader in the experiment than in the model, implying that significant Pb off centering exists already at 650 K. Egami *et al.* [20] also proposed Pb off centering in PMN above the Burns temperature based on similarities between the temperature dependencies of the Pb displacements in various Pb containing perovskites and the normalized Raman intensity of $Pb(Mg_{1/3}Ta_{2/3})O_3$ by Siny and Smirnova [21]. Thus, the gradual development of a shoulder around ~2.5 Å at lower temperatures is mainly due to a decrease of thermal vibrations.

Below room temperature [Fig. 1(b)] the experimental PDFs reveal a more interesting structure. First, the Mg/Nb-O peak around 2.02 Å splits into two peaks, suggesting local Mg/Nb displacements along the ⟨111⟩ direction. Note that this peak shows almost no temperature dependence between 250 and 15 K, consistent with Nb K-edge EXAFS measurements [12]. In general, PDF peaks become sharper with decreasing temperature due to decreasing thermal motion. Thus, this temperature dependence suggests an increasing distribution of Mg/Nb displacements with decreasing temperature. Second, the Pb-O peak around 2.85 Å now splits into three peaks at ~2.45, 2.85, and 3.33 Å. Third, the Pb-Mg/Nb peak around 3.5 Å splits into two Pb-Mg/Nb bonds at ~3.33 and 3.64 Å mostly due to the displacement of Pb ions. Thus, the peak around 3.3 Å has both Pb-O and Pb-Mg/Nb components. The splitting of the Pb-Mg/Nb peak below room temperature suggests that the Pb ions are locally shifted along ⟨100⟩ against Mg/Nb. However, local ⟨100⟩ shifts are correlated in the medium range, and on average Pb ions shift along ⟨111⟩ as discussed below. Interestingly, the peak around 4.05 Å (lattice constant of PMN) is well defined; thus, the overall lattice parameter is maintained although ions are strongly displaced from their high symmetry positions.

We now address the medium-range correlations (PNRs) between these local atomic displacements. Figure 2(a) shows the PDF spectra from 1000 to 15 K in the r range up to 16 Å, and Fig. 2(b) shows the temperature dependence of the peak intensities in the doublet between 8.0 Å $< r < 9.8$ Å. Here both peaks have contributions from almost all possible ionic pairs. The solid line is the calculated temperature dependence of the peak height using the average Pb, Mg/Nb, and O thermal parameters
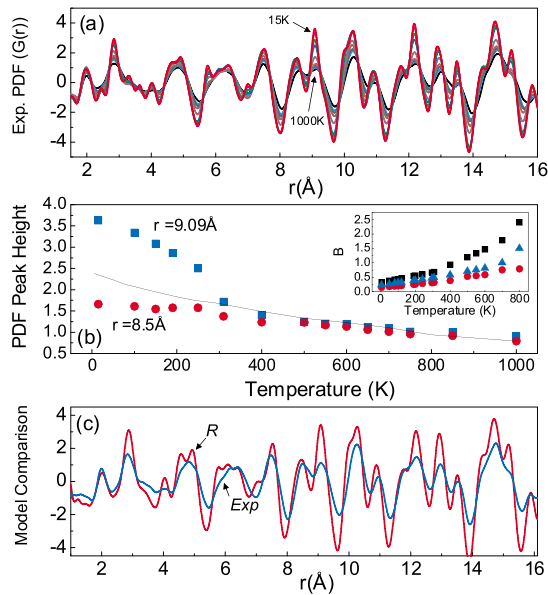
FIG. 2 (color). (a) Temperature dependence of the PDF spectra of PMN at temperatures $T = 1000, 750, 650, 500, 313, 250, 190, 100,$ and 15 K. All PDFs were obtained with $Q_{max} = 25$ Å^{-1}. (b) PDF peak height in the doublet between 8.0 Å $< r < 9.8$ Å as a function of temperature. The line is the expected average PDF peak height using the thermal parameters in the inset. The inset shows the thermal parameters of Pb (squares), Mg/Nb (circles), and O (triangles) [22]. (c) Comparison of rhombohedral (R model) PDF (R) with the experimental PDF (Exp) at 650 K.

from Bonneau *et al.* [22], which are reproduced in the inset. Note the strong deviation of the data below $T \sim 250$ K, an indication of PNRs. This result is consistent with ^{207}Pb nuclear-magnetic-resonance (NMR) measurements by Blinc *et al.* [23], which show a sudden increase of the intensity of the polar cluster line below 210 K due to Pb displacement along the [111] direction, both in-field cooled and zero-field cooled ^{207}Pb NMR spectra. Neutron scattering measurements by Wakimoto *et al.* [24] also suggest the presence of PNRs with a stable local spontaneous polarization below $T \sim 220$ K.

We modeled the PNRs using rhombohedral symmetry (R model: space group $R3m$), wherein the Pb, Mg/Nb, and oxygen octahedra are displaced along the $\langle 111 \rangle$ directions, assuming rigid oxygen octahedra. Similar models of rhombohedral correlations with $\langle 111 \rangle$ atomic displacements [23,25,26] and noncollinear $\langle 100 \rangle$ displacements that average to rhombohedral symmetry [27] have been proposed in $Pb(Mg_{1/3}Nb_{2/3})O_3$ and $Pb(Sc_{1/2}Ta_{1/2})O_3$, respectively. Attempts to model our data using displacements of orthorhombic symmetry (with Pb, Mg/Nb ions, and oxygen octahedra displaced along $\langle 110 \rangle$ directions with the same magnitudes as in the rhombohedral model) were unsuccessful, with some PDF peaks being too strong and others too weak.

In Fig. 2(c) we compare the R model PDF with the experimental PDF at 650 K. For the R model PDF calcu-

lation the thermal parameters were taken from Bonneau *et al.* [22], and the following atomic positions were used, determined to best simulate the differences between low-temperature PDFs and the PDF at 650 K: Pb $(-0.0454, -0.0454, -0.0454)$ and O $(0.5246, 0.5246, 0.0246)$ with Mg/Nb position fixed.

The PDF peaks of the R phase are quite distinct from those at 650 K. In fact, the relative intensities of the PDF peaks in the R phase and at 650 K resemble the low-temperature and high-temperature end members shown in Fig. 2(a), respectively. Therefore, if we assume that PNRs are dispersed in a pseudocubic host lattice [23,25], growing in size and volume fraction with decreasing temperature, we expect that features of the R model PDF will become more evident with decreasing temperature. This is exactly what we observe in the experimental PDFs shown in Fig. 2(a).

The volume fraction of the PNRs was estimated using a simple model PDF: $G_m = \alpha(T)G_R + [1 - \alpha(T)]G_{PC}$, where G_R and G_{PC} are the rhombohedral and the host pseudocubic (PC) model PDFs, respectively, and $\alpha(T)$ is the volume fraction of the rhombohedral phase as a function of temperature. For the R model PDF calculations the atomic coordinates given above were used for all temperatures. For the host phase, ^{93}Nb NMR measurements of PMN by Laguta *et al.* [28] suggest that the ions are locally displaced from their high symmetry cubic position above the maximum temperature of the permittivity. Therefore, we first introduced ionic displacements in a $10 \times 10 \times 10$ unit cell via a reverse Monte Carlo fit to the experimental PDF at 650 K, using the DISCUS program [29]. These ionic displacements were then fixed, and the PC model PDF was calculated at various temperatures using the thermal parameters from Bonneau *et al.* [22]. (The same thermal parameters are used for both cubic and rhombohedral phases.) After calculating both pseudocubic and rhombohedral PDFs at a given temperature, $\alpha(T)$ was adjusted to obtain the best match to the corresponding experimental PDF. Figures 3(a)–3(c) show these comparisons at 500, 250, and 50 K in the r range up to $r = 16$ Å. Considering the simplicity of the model PDF calculations, the overall agreement at various temperatures is very good.

In Fig. 3(d) we show the temperature dependence of $\alpha(T)$, along with the correlation length of local polarization determined by Xu *et al.*, using neutron elastic diffuse scattering [30], shown in the inset. The volume fraction steadily increases with decreasing temperature, reaching $\sim 30\%$ at 15 K. This estimation is consistent with the value obtained by Mathan *et al.* at 5 K [25]. The correlation length ξ of local polarization shows a sharp increase from $\xi \sim 15$ to $\xi \sim 60$ Å around $T \sim 200$ K. Note that around $T \sim 200$ K, where the correlation length drastically increases, $\alpha(T)$ reaches the percolation threshold $P_c \sim 28\%$ for spherical objects in three dimensions [31]. This implies that, as the volume fraction of the PNR increases, PNRs get closer and start to overlap with each other below
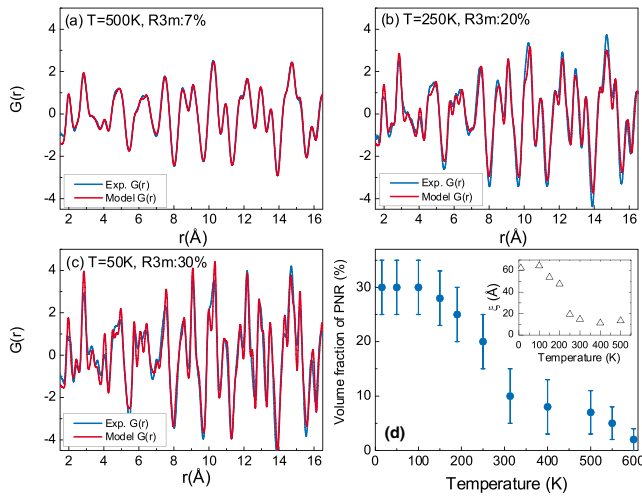
FIG. 3 (color). Comparison of the "two-phase" model PDF with the experimental PDFs at (a) $T = 500$ K, (b) $T = 250$ K, and (c) $T = 50$ K. The model PDF is calculated from $G_m = \alpha(T)G_R + [1 - \alpha(T)]G_{PC}$, where G_R and G_{PC} are model PDFs for the rhombohedral and the pseudocubic phases. $\alpha(T)$ is the volume fraction of the rhombohedral phase. (d) The volume fraction increases with decreasing temperature, reaching 30% at 15 K. The inset shows the correlation length of local polarization as a function of the temperature (taken from Xu et al. [30]).

$T \sim 200$ K. This percolation temperature correlates well with the abrupt increase in the correlation length of local polarization to $\xi \sim 50\text{--}60$ Å, determined independently [30]. Because of the random field generated by a random distribution of Mg^{2+}/Nb^{5+} ions, the PNRs are frozen [32,33] and do not grow beyond 60 Å. In an applied electric field, however, the polarizations in the separate PNRs are aligned, and the separate PNRs form a macropolar domain. Once the macropolar domain is formed, the dipoles in the domain do not randomly orient even after the electric field is turned off.

This picture helps to explain some basic behavior found in PMN, such as hysteresis in the field-induced polarization [34], the field-induced rhombohedral phase transition below 220 K [35], and the anomaly in the dielectric permittivity near 212 K upon field heating after zero-field cooling [7]. Our measurements, therefore, provide direct local structural evidence for the importance of percolating PNRs in explaining many features of the relaxor behavior found in PMN below the Burns temperature.

*Electronic address: jeong@lanl.gov
[1] G. A. Smolenskii and A. I. Agranovskaia, Sov. Phys. Tech. Phys. **3**, 1380 (1958).
[2] K. Binder and A. P. Young, Rev. Mod. Phys. **58**, 801 (1986).
[3] L. E. Cross, Ferroelectrics **76**, 241 (1987).
[4] G. A. Samara, J. Phys. Condens. Matter **15**, R367 (2003).
[5] D. Viehland et al., Phys. Rev. B **43**, 8316 (1991).
[6] E. V. Colla et al., Phys. Rev. Lett. **74**, 1681 (1995).
[7] V. Westphal, W. Kleemann, and M. D. Glinchuk, Phys. Rev. Lett. **68**, 847 (1992).
[8] H. You and Q. M. Zhang, Phys. Rev. Lett. **79**, 3950 (1997).
[9] P. M. Gehring et al., Phys. Rev. Lett. **87**, 277601 (2001).
[10] G. Burns and F. H. Dacol, Solid State Commun. **48**, 853 (1983).
[11] J. Zhao et al., Appl. Phys. Lett. **72**, 1048 (1998).
[12] E. Prouzet et al., J. Phys. Condens. Matter **5**, 4889 (1993).
[13] I.-W. Chen, P. Li, and Y. Wang, J. Phys. Chem. Solids **57**, 1525 (1996).
[14] T. Egami, H. D. Rosenfeld, B. H. Toby, and A. Bhalla, Ferroelectrics **120**, 11 (1991).
[15] H. D. Rosenfeld and T. Egami, Ferroelectrics **150**, 183 (1993).
[16] Th. Proffen and S. J. L. Billinge, J. Appl. Crystallogr. **32**, 572 (1999).
[17] T. Egami and S. J. L. Billinge, *Underneath the Bragg Peaks: Structural Analysis of Complex Materials* (Pergamon Press, Oxford, UK, 2003).
[18] I.-K. Jeong et al., Phys. Rev. B **63**, 205202 (2001).
[19] I.-K. Jeong et al., J. Phys. Chem. A **103**, 921 (1999).
[20] T. Egami, E. Mamontov, W. Dmowski, and S. B. Vakhrushev, in *Fundamental Physics of Ferroelectrics*, edited by Peter K. Davies and David J. Singh, AIP Conf. Proc. No. 677 (AIP, New York, 2003), p. 48.
[21] I. G. Siny and T. A. Smirnova, Ferroelectrics **90**, 191 (1989).
[22] P. Bonneau et al., J. Solid State Chem. **91**, 350 (1991).
[23] R. Blinc, V. Laguta, and B. Zalar, Phys. Rev. Lett. **91**, 247601 (2003).
[24] S. Wakimoto et al., Phys. Rev. B **65**, 172105 (2002).
[25] N. de Mathan et al., J. Phys. Condens. Matter **3**, 8159 (1991).
[26] N. Takesue, Y. Fujii, and H. You, Phys. Rev. B **64**, 184112 (2001).
[27] W. Dmowski, M. K. Akbas, P. K. Davies, and T. Egami, J. Phys. Chem. Solids **61**, 229 (2000).
[28] V. V. Laguta et al., Phys. Rev. B **67**, 104106 (2003).
[29] Th. Proffen and R. Neder, J. Appl. Crystallogr. **30**, 171 (1997).
[30] G. Xu, G. Shirane, J. R. D. Copley, and P. M. Gehring, Phys. Rev. B **69**, 064112 (2004).
[31] E. J. Garboczi et al., Phys. Rev. E **52**, 819 (1995).
[32] Z.-G. Ye et al., Phys. Rev. B **67**, 104104 (2003).
[33] A. A. Bokov, Fiz. Tverd. Tela (St. Petersburg) **36**, 36 (1994).
[34] V. A. Bokov and I. E. Myl'nikova, Sov. Phys. Solid State **3**, 613 (1961).
[35] G. Calvarin, E. Husson, and Z. G. Ye, Ferroelectrics **165**, 349 (1995).